

# Investigations on the Powerslide of Automobiles

Johannes Edelmann<sup>1</sup>, Manfred Plöchl<sup>1</sup>, Peter Lugner<sup>1</sup>, Werner Mack<sup>1</sup> and Anton Falkner<sup>2</sup>

<sup>1</sup>Division of Vehicle System Dynamics and Biomechanics,  
 Institute of Mechanics and Mechatronics,  
 Vienna University of Technology, Vienna, Austria  
<sup>2</sup>Integrated Vehicle Validation, MAGNA STEYR Fahrzeugtechnik,  
 Graz, Austria

Vienna University of Technology  
 Institute of Mechanics and Mechatronics  
 Wiedner Hauptstraße 8-10 / E325 / A1  
 1040 Wien, Austria  
 Phone: +43 1 58801 32525  
 Fax: +43 1 58801 32599  
 E-mail: manfred.ploechl@tuwien.ac.at

Under regular steady-state cornering conditions, only small vehicle sideslip angles appear. However, in rallye sports cornering manoeuvres are often performed with large vehicle sideslip angles via powerslides. The presented investigations explain the corresponding phenomena in relation to regular driving conditions. Starting with test runs of a sports utility vehicle with rear-wheel drive on watered asphalt, the measurement results are compared to results from theoretical investigations. To this aim, the equations of motion of a basic nonlinear vehicle model and a tyre model that comprises the mutual influence of the lateral and longitudinal tyre forces are employed to find multiple steady-state driving conditions including the powerslide solution. The stability of these solutions is investigated using analytical methods.

Topics / Vehicle Dynamics

## 1. INTRODUCTION

Besides steady-state cornering as common in every day driving, drifting or powerslide through the curve especially on low friction surfaces is possible and practised in rallye sports. This kind of cornering is characterized by large sideslip angles, a negative steering angle and an essential influence of the traction force on the driving condition. In figures 1 and 2, the principal driv-

ing condition of powerslide is demonstrated with a two-wheel vehicle model, and a possible steady-state diagram characterizes the situation.

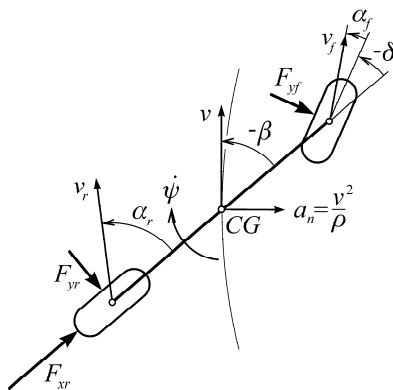


Fig. 1 Powerslide driving condition for rear-wheel drive

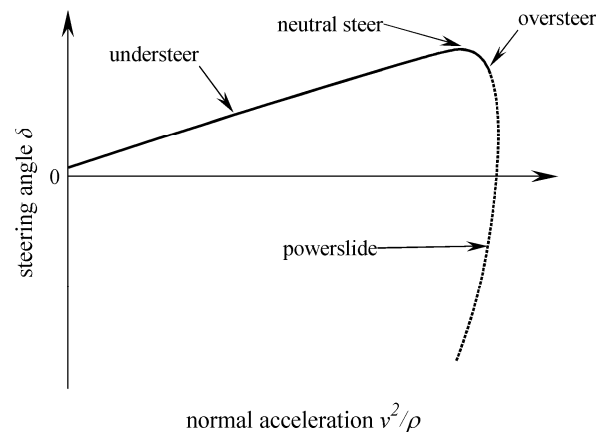


Fig. 2 Steady-state steering characteristics

Though steady-state cornering conditions are well studied including nonlinear vehicle and tyre descriptions with respect to steering characteristics, e.g. in very early substantial contributions by Pacejka, Lugner or more

recent works by Guo and Winkler, these extraordinary conditions have however not been investigated [1-3],[4],[5],[6]. Nevertheless, Pacejka and Laurence et al. presented conditions which show also negative steering angle characteristics, see figure 2, that can be interpreted as powerslide [1],[7]. However, these investigations only have been performed for small sideslip angles. Using a nonlinear vehicle model, Hasselgruber found different steady-state solutions within a limited velocity range [8]. A detailed compendium is given by Pacejka [9].

Since the powerslide is a very special driving condition, it is the intention of the investigation to start with experimental measurements of the powerslide, showing the existence of this kind of steady-state driving conditions for a specific vehicle, and to verify that these conditions are steady-state and to interpret the measurements by simulation.

**2. MEASUREMENTS**

The field tests were performed with a sports utility vehicle (SUV), figure 3, on watered asphalt on a circular path with a radius of  $\rho=50$  m. Rear wheel drive was realised by deactivating the all wheel drive system; the electronic stability system has also been deactivated. The main vehicle parameters are summarized in table 1.



Fig. 3 SUV test vehicle performing a powerslide

Table 1 Vehicle parameters

vehicle mass	$m$	2066	kg
yaw moment of inertia	$I_z$	3120	kgm <sup>2</sup>
front axle location from CG	$l_f$	1.304	m
rear axle location from CG	$l_r$	1.489	m
CG position over ground	$h$	0.660	m
wheel track	$s$	1.540	m
front suspension rate	$c_f$	60700	N/m
rear suspension rate	$c_r$	43500	N/m

A time record of the steering angle  $\delta$ , the vehicle sideslip angle  $\beta$  (from two independent measuring systems) and the vehicle's velocity  $v$  are given in figure 4 as an example of a powerslide measurement test run.

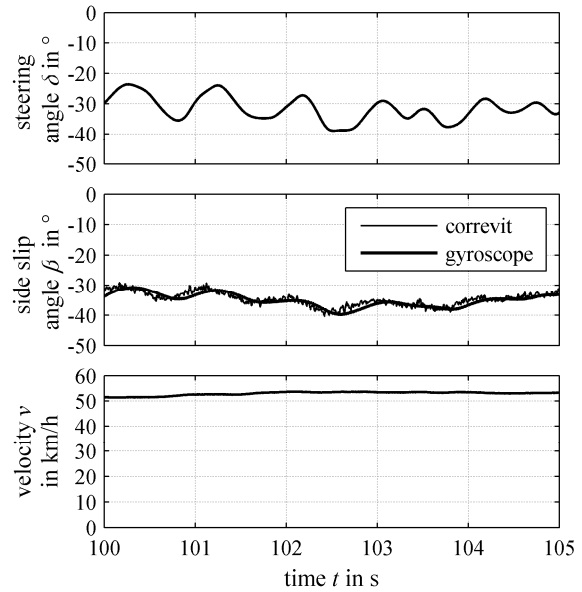


Fig. 4 Powerslide measurement

The steering angle is calculated from the measured steering wheel angle considering a nonlinear steering ratio characteristic. At nearly constant velocity, only small changes in the sideslip angle occur, indicating an overall steady-state driving condition. However, in this case obviously a permanent correction from the driver around a mean steering angle is necessary, a behaviour that was not noticed for non-powerslide conditions, where the steering angle does not vary substantially. Consequently, two questions arise: Which steady-state conditions are possible? Are the steady-state points stable? This is obviously not the case for the measurements presented in figure 4.

By calculating the means of the signals from a 'steady-state' run, the measurements of different steady-state driving conditions are presented in figure 5

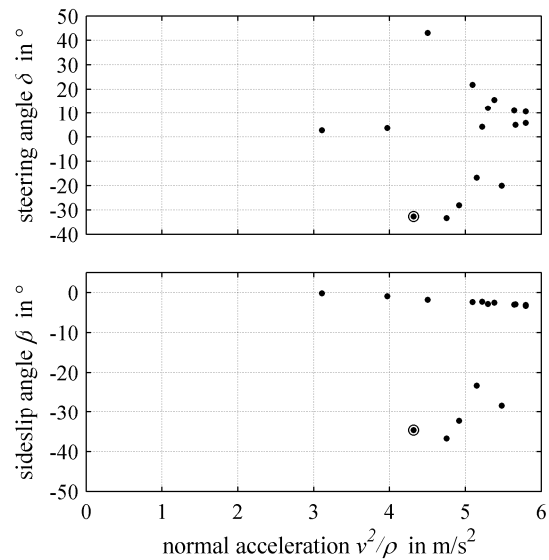


Fig. 5 Measured steady-state handling characteristics

with the vehicle sideslip angle  $\beta$  taken from the correvit system; the steady-state point resulting from the run shown in figure 4 is encircled.

### 3. VEHICLE MODEL

To interpret the measurements, a nonlinear basic four-wheel vehicle model is introduced to allow for high lateral accelerations, and which is not limited to small steering angles  $\delta_1$  and  $\delta_2$  of the front wheels or small sideslip angles  $\beta$  of the vehicle, figure 6. Consequently, also the sideslip angles  $\alpha_i$  ( $i = 1-4$ ) of the wheels can be

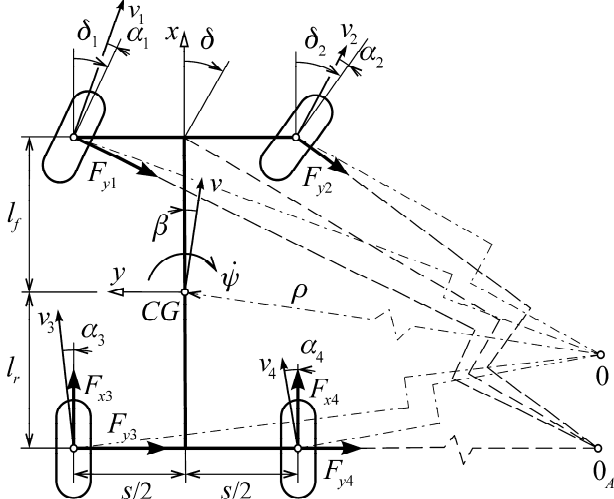


Fig. 6 Vehicle model at regular driving condition

large. From geometric and kinematical considerations, one derives the nonlinear relations

$$\begin{aligned} \tan(\delta_1 - \alpha_1) &= \frac{v \sin \beta + l_f \dot{\psi}}{v \cos \beta + \dot{\psi} s/2}, \\ \tan(\delta_2 - \alpha_2) &= \frac{v \sin \beta + l_f \dot{\psi}}{v \cos \beta - \dot{\psi} s/2}, \\ \tan \alpha_3 &= \frac{l_r \dot{\psi} - v \sin \beta}{v \cos \beta + \dot{\psi} s/2}, \\ \tan \alpha_4 &= \frac{l_r \dot{\psi} - v \sin \beta}{v \cos \beta - \dot{\psi} s/2} \end{aligned} \quad (1)$$

and

$$\begin{aligned} \frac{(l_f + l_r)}{\tan \delta_1} &= \frac{(l_f + l_r)}{\tan \delta} + \frac{s}{2}, \\ \frac{(l_f + l_r)}{\tan \delta_2} &= \frac{(l_f + l_r)}{\tan \delta} - \frac{s}{2}, \end{aligned} \quad (2)$$

to realize Ackermann steering behaviour, with the Ackermann front wheel steering angle  $\delta$  and yaw angle velocity  $\dot{\psi}$ .

The derivation of the equations of motion is straightforward. Having the possibility to investigate the stability of the motion by calculating the eigenvalues of

the linearized system in mind, these equations are formulated including longitudinal and yaw acceleration (neglecting roll, pitch and heave motion and assuming small roll and pitch angles). Newton's law and Euler's equations yield

$$\begin{aligned} m\dot{v} \cos \beta - mv(\dot{\beta} + \dot{\psi}) \sin \beta &= F_{x3} + F_{x4} - F_{y1} \sin \delta_1 - F_{y2} \sin \delta_2, \\ m\dot{v} \sin \beta + mv(\dot{\beta} + \dot{\psi}) \cos \beta &= F_{y1} \cos \delta_1 + F_{y2} \cos \delta_2 + F_{y3} + F_{y4}, \\ 0 &= F_{z1} + F_{z2} + F_{z3} + F_{z4} - mg, \\ 0 &= (F_{z1} - F_{z2} + F_{z3} - F_{z4}) s/2 - (F_{y1} \cos \delta_1 + F_{y2} \cos \delta_2 + F_{y3} + F_{y4}) h, \\ 0 &= -(F_{z1} + F_{z2}) l_f + (F_{z3} + F_{z4}) l_r + (F_{y1} \sin \delta_1 + F_{y2} \sin \delta_2 - F_{x3} - F_{x4}) h, \\ I_z \ddot{\psi} &= (-F_{y1} \sin \delta_1 + F_{y2} \sin \delta_2 + F_{x3} - F_{x4}) s/2 + (F_{y1} \cos \delta_1 + F_{y2} \cos \delta_2) l_f - (F_{y3} + F_{y4}) l_r. \end{aligned} \quad (3)$$

$F_{xi}$ ,  $F_{yi}$  mean the lateral and longitudinal tyre forces,  $F_{zi}$  are the vertical tyre forces. Since only low velocities up to 60 km/h appear and no vehicle specific parameters are available, the aerodynamic properties are disregarded, as well as the tyre rolling resistance.

Assuming both a linear relation between the deflections  $\Delta z_i$  and the corresponding deflections  $\Delta z_i$  and the geometric constraint  $(\Delta z_1 + \Delta z_4) = (\Delta z_2 + \Delta z_3)$  leads to

$$(F_{z1} - F_{z2}) c_r = (F_{z3} - F_{z4}) c_f. \quad (5)$$

The roll stiffness of the front and rear torsion bars is included in the front and rear suspension rates  $c_f$ ,  $c_r$ . The effect of the rear differential gear yields

$$F_{x3} = F_{x4} =: F_x. \quad (6)$$

To consider higher longitudinal forces at the driven rear wheels and large sideslip angles, a complex tyre characteristics description is required. Because of the rear-wheel drive, the front lateral tyre forces  $F_{yi}$  ( $i=1,2$ ) only depend on the corresponding side slip angles and the wheel loads,

$$F_{y1} = F_{y1}(\alpha_1, F_{z1}), \quad F_{y2} = F_{y2}(\alpha_2, F_{z2}), \quad (7)$$

whereas the rear lateral tyre forces  $F_{yi}$  ( $i=3,4$ ) additionally depend on the longitudinal tyre forces:

$$F_{y3} = F_{y3}(\alpha_3, F_x, F_{z3}), \quad F_{y4} = F_{y4}(\alpha_4, F_x, F_{z4}). \quad (8)$$

The applied steady-state tyre characteristics are shown in figure 7 with an estimated maximum force coefficient

$\mu_{max}=0.65$  (for a given nominal vertical tyre force  $F_{z,nom}=5800$  N) and a sliding coefficient of friction  $\mu_g=0.59$  representing tyre – wet asphalt contact conditions. For details refer to Kortüm et al. [10].

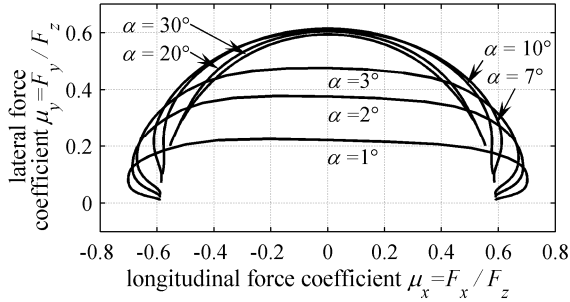


Fig. 7 Steady-state tyre characteristics

The steady-state solutions (indicated below with index 0) of the above set of equations are found by setting

$$\dot{v} = 0, \quad \dot{\psi} = 0, \quad \dot{\beta} = 0, \quad \dot{\psi} = \frac{v}{\rho}, \quad (9)$$

with the constant curvature  $1/\rho$ .

For stability analysis, equations (1)-(8) are linearized with respect to the state variables  $\dot{\psi}$ ,  $\beta$  and  $v$  and the input variables  $\delta$  and  $F_x$  at the steady-state solutions by setting

$$\begin{aligned} \dot{\psi} &= \dot{\psi}_0 + \Delta\dot{\psi}, \quad \beta = \beta_0 + \Delta\beta, \quad v = v_0 + \Delta v, \\ \delta &= \delta_0 + \Delta\delta, \quad F_x = F_{x0} + \Delta F_x, \end{aligned} \quad (10)$$

with small deviations indicated by  $\Delta$ . This leads to

$$\Delta\dot{\underline{x}} = \mathbf{A}\Delta\underline{x} + \mathbf{B}\Delta\underline{u} \quad (11)$$

with the state vector  $\Delta\underline{x} = [\Delta\dot{\psi}, \Delta\beta, \Delta v]^T$  and the input vector  $\Delta\underline{u} = [\Delta\delta, \Delta F_x]^T$ . The eigenvalues  $\lambda_i$  ( $i=1-3$ ) are derived from  $\det(\mathbf{A} - \lambda\mathbf{I}) = 0$ .

#### 4. RESULTS

Using the parameters from table 1 and the tyre characteristics shown in figure 7, the steady-state characteristics of the vehicle model are calculated by numerically solving equations (1)-(8) using (9) with a given radius  $\rho=50$  m following the field tests.

The nonlinear set of equations yields up to four steady-state solutions, see figure 8. The full lines represent sections for both regular and powerslide steady-state driving conditions; solutions illustrated by dotted lines are not addressed here any further. The additionally inserted measurement results match well to the analytical findings, even though there are some differences in the powerslide solution, resulting from the limitations of the vehicle model and the tyre characteristics approximation.

These results already indicate that some of the solution sections will be associated with unstable vehicle behaviour, which becomes obvious from the measurements shown in figure 4.

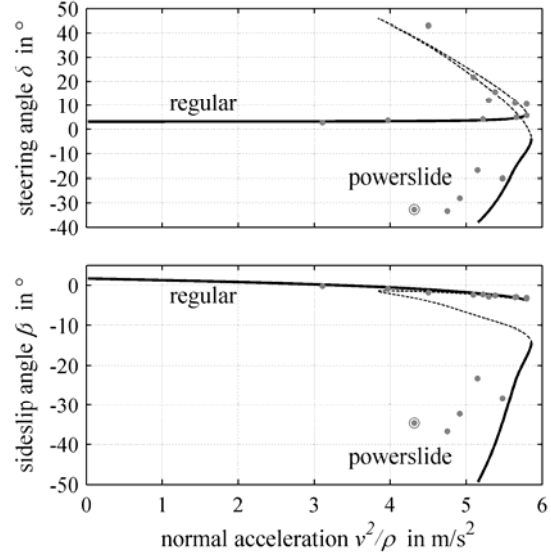


Fig. 8 Simulated steady-state handling characteristics and corresponding measurements, marked with dots

Consequently, the root locus depending on  $v$  of the linearized equations of motion (11) is investigated, figure 9. The full and dotted lines correspond to the sections as introduced in figure 8.

The three eigenvalues start - within a respective section - for the lowest vehicle velocity  $v$  at the x-marks, the highest velocity is reached at the o-marks. One of the

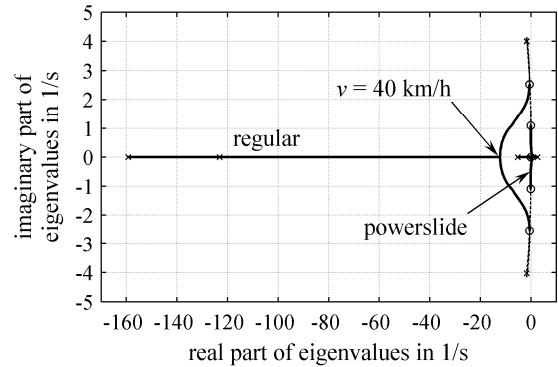


Fig. 9 Root locus depending on  $v$

three eigenvalues is a real negative number close to zero (about  $-0.1$  1/s) for all sections. By investigating the associated eigenvector of the negative eigenvalue, it turns out that it has a nearly exclusive component for the vehicle's velocity. Under regular driving conditions, the two eigenvectors associated with the two other eigenvalues, which become complex at a velocity of approximately 40 km/h, have mainly components for the yaw rate and sideslip angle, but a smaller component for the vehicle's velocity.

Since the two steady-state solutions with large posi-

tive steering angles (dotted lines in figures 8 and 9) are not investigated here, only the powerslide section is presented in more detail, figure 10. Starting unstable with a positive real eigenvalue at velocity  $v=57$  km/h corresponding to a lateral acceleration of about  $5.2$  m/s<sup>2</sup> (lowest point in curves of figure 8), an increase of velocity yields complex eigenvalues at a vehicle velocity of  $61.4$  km/h and finally - only  $0.1$  km/h below the maximum velocity - leads to stable powerslide conditions. That means, only a very small velocity range corresponds to a stable steady-state powerslide range of the investigated vehicle! The above mentioned, negative real eigenvalue close to zero is also marked in figure 10.

Considering the eigenvectors corresponding to the two significantly varying eigenvalues, the components for the velocity in the case of powerslide are considerably higher than under regular driving conditions.

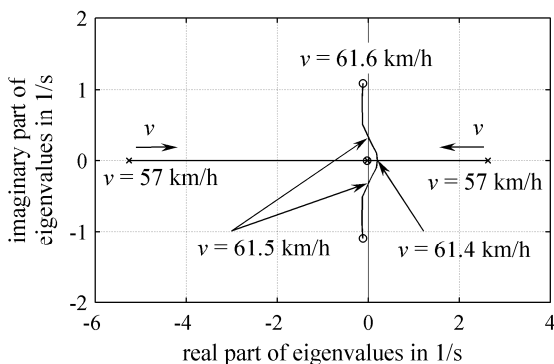


Fig. 10 Root locus depending on  $v$ , powerslide detail corresponding to figure 9

The theoretical investigation reveals that the measured powerslide driving condition presented in figure 4 is unstable and explains the necessity of a permanent steering (and throttle) correction to stabilize the vehicle.

In figure 11 the required simulated longitudinal tyre forces for steady-state regular driving and powersliding are plotted with full lines. Comparing the differences between simulation results and measurements in the powerslide section of figure 8, it becomes evident that the longitudinal tyre forces appearing during the test runs have to be less than those presented in figure 11. However, the necessity for deactivating the all wheel drive system at the used test vehicle to provide higher rear traction forces to perform powerslide driv-

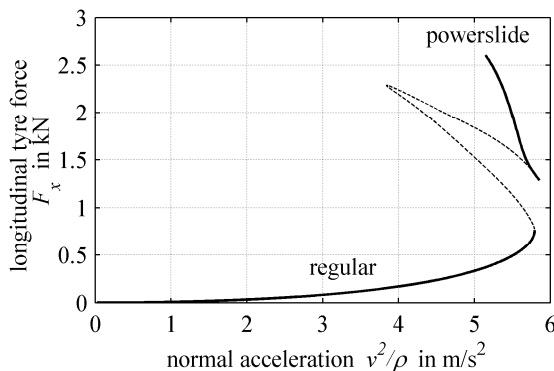


Fig. 11 Longitudinal tyre force of driven rear wheels

ing manoeuvres on watered asphalt becomes obvious.

## 5. CONCLUSIONS

By applying a simplified nonlinear vehicle model, taking into account large possible sideslip and steering angles and nonlinear tyre characteristics, it has been shown theoretically that at specific vehicle velocities several steering angles with corresponding vehicle sideslip angles are possible for steady-state cornering.

One section of these steady-state solutions is characterized by a large vehicle sideslip angle and a negative steering angle and is referred to as powerslide driving condition. To meet this driving condition considerable large traction forces are essential. The theoretical results have been validated by field tests on wet asphalt.

Both theoretical and experimental investigations have revealed that the steady-state powerslide is unstable at nearly all respective velocities.

A more detailed insight into nonlinear handling characteristics including the powerslide will be published in a forthcoming paper.

## REFERENCES

- [1] Pacejka, H. B. "Simplified analysis of steady-state turning behaviour of motor vehicles. Part1. Handling diagrams of simple systems", *Vehicle System Dynamics* **2**, 1973, pp. 161-172.
- [2] Pacejka, H. B. "Simplified analysis of steady-state turning behaviour of motor vehicles. Part2. Stability of the steady-state turn", *Vehicle System Dynamics* **2**, 1973, pp. 173-183.
- [3] Pacejka, H. B. "Simplified analysis of steady-state turning behaviour of motor vehicles. Part3. More elaborate systems", *Vehicle System Dynamics* **2**, 1973, pp. 184-204.
- [4] Lugner, P. "Zur Stabilität der Kurvenfahrt eines Kraftfahrzeuges mit und ohne Tangentialbeschleunigung", *Vehicle System Dynamics* **1**, 1972, pp. 17-36, in German.
- [5] Guo, K. H. "A Study on a Phase Plane Representation for Identifying Vehicle Behavior", *Vehicle System Dynamics Supplement* **15**, 1986, pp. 152-167.
- [6] Winkler, C. B. "Simplified Analysis of the Steady-State Turning of Complex Vehicles", *Vehicle System Dynamics* **29**, 1998, pp. 141-180.
- [7] Laurence, P., Basset, M., Coutant, P. and Gissinger, G. "Lateral Vehicle Behaviour: Comparison of Subjective/Objective Assessment Using the Choquet Integral", *Vehicle System Dynamics* **34**, 2000, pp. 357-379.
- [8] Hasselgruber, H. "Fahrzustand und Stabilitätsverhalten des Kraftfahrzeuges bei Kurvenfahrt", *Forschung im Ingenieurwesen* **30**, 1964, pp. 145-155, in German.
- [9] Pacejka, H. B. "Tyre and Vehicle Dynamics" (Oxford: Butterworth-Heinemann), 2002.
- [10] Kortüm, W., Lugner, P. "Systemdynamik und Regelung von Fahrzeugen" (Berlin: Springer Verlag), 1994, in German.